Numerical Analysis of Concrete Overlays on Flexible Pavements

Fereidoon Moghaddas Nejad[1], Sepehr Ghafari[2]

Abstract

Due to the proven durability and long-term performance of Portland cement concrete (PCC) surfaces, rehabilitation of hot-mix asphalt (HMA) pavements with PCC overlays has been widely considered in the past 15 years (Cable 2005). In this study, a number of finite element models of conventional HMA pavements overlaid by a jointed plain concrete pavement (JPCP) were analyzed to measure and assess the effects of asphalt layer and concrete slab thickness variations, as well as changes in the asphalt layer and subgrade mechanical properties, on the service life of the overlaid pavement.

Introduction

The ANSYS finite element software suite was used to model and analyze the pavement system. The Asphalt concrete was modeled as a Maxwell viscoelastic material, and the nonlinear behavior of subgrade, base, and subbase layers were modeled using the Drucker-Prager material model. The concrete and the steel dowel and tie bars were considered to behave linearly elastically to conserve in computational time and expense. Various axle loads and configurations are considered; therefore, computationally intensive three-dimensional models were necessary to account for the interaction between tires.

The allowable number of load repetitions based on criteria for fatigue in the concrete and fatigue cracking in the asphalt layer, as well as permanent deformation, are calculated for each model. Consequently, depending on subgrade, asphalt and concrete properties, the design thickness of a JPCP overlay can be determined using the graphs and equations presented.

Case Study

Prior to the analysis of the overlay system that can actually be considered as a composite pavement system, steps were taken to verify the applicability of the elements and the modeling techniques chosen for the analysis of the composite pavement. A three-dimensional finite element model of the rigid runway pavement at Denver International Airport was developed, and the results obtained from the analysis were compared with the instrumentation results presented by the FAA and the results obtained from the analysis with NIKE3D finite element software.

---

[1] Deputy for Research, Transportation Research Institute, No.19, Noor Street, Africa Blvd., Tehran, Iran and Assistant Professor, PhD, Dept. of Civil and Environmental Engineering, Amirkabir University of Technology, Tehran Hafez Ave., Iran. Fax & Tel.: +98 21 22549358. E-mail: f.moghadas@yahoo.com.

[2] MSc, Dept. of Civil and Environmental Engineering, Amirkabir University of Technology, Tehran Hafez Ave., Iran. Fax & Tel.:+98 912 1496991. E-mail: sepehr_g@aut.ac.ir.

Eight-node brick elements and interface elements were used in modeling the rigid pavement (ANSYS, Inc. 1999). Material properties, and layer and slab dimensions are as summarized in Table 1. The load data are also given in Table 2. It should be noted that a Boeing-777 loading was used in the analysis.

Table 1. Layer and material properties used in the analysis (David 1998)

Variable	PCC slab	Base layer	Subgrade
Young's modulus E	27600 MPa	3450 MPa	103.5 MPa
Poisson's ratio	0.15	0.20	0.40
Thickness	356 mm	203 mm	N.A.
Cutoff depth	N.A.	N.A.	38100 mm
Joint stiffess	45454.5 kg/mm/mm	N.A.	N.A.

Table 2. Loading data for Boeing 777 and Boeing 727 (David 1998)

Aircraft	Gross Weight, kg	Percent of Gross Weight on Main Gear	Number of Wheels in Gear	Individual Wheel Load, kg	Contact Pressure, MPa
B-777	309091	95	6	24470	14.8

Figure 1 compares the computed static distribution of strain along the longitudinal loaded slab edge, in this study, to the strain recorded at the relevant strain gauges in the field as well as the strain obtained from NIKE3D finite element model.
A comparison between maximum tensile strain and slab deflections is also presented in Table 3.

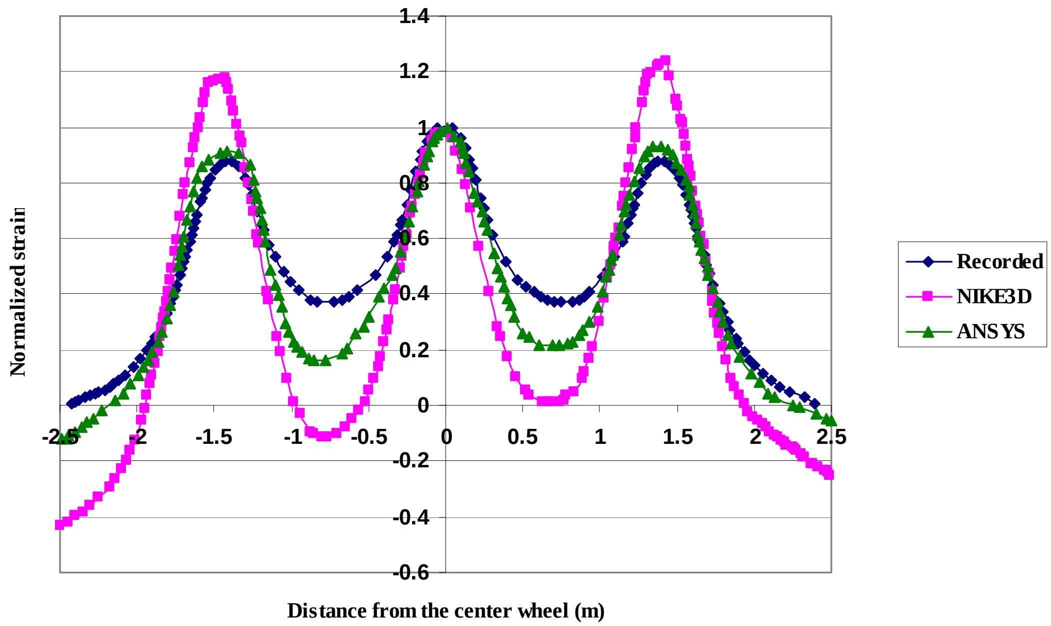

Figure 1. Comparison between computed and recorded strains

Table 3. Comparison between deflections and strains

Output	ANSYS	NIKE3D	Recorded
Maximum tensile strain at the bottom of the loaded slab (10^{-6})	29.30	40.30	17.41
Maximum slab deflection (mm)	2.873	2.700	2.775

Pavement material properties and the finite element model

The elastic material properties of the modeled pavement layers used in this research are provided in Table 4. As can be seen, the concrete in the overlay layer and the steel used in the dowel and tie bars are assumed to behave linearly elastically. The HMA was considered to be a viscoelastic material. equations 1 and 2 express the shear relaxation modulus and the corresponding bulk modulus for the model, where R_n = elastic spring constants and η_n = viscosity constants of the generalized Maxwell model. The shear relaxation modulus and bulk modulus are related through the Poisson's ratio $\upsilon(t)$ as shown in equation 3 The long-term and instantaneous moduli can be obtained from equations 4 to 7. From primary mechanics, the hear and bulk moduli are obtained from equations 8 and 9. The viscoelastic properties of the HMA layer were determined using equations 1 to 9, which present a generalized Maxwell model (Abbas 2004, Johnson 2007, Ullidtz 1987), and are given in Table 5. The nonlinear behavior of base, subbase, and subgrade were simulated using Drucker-Prager material model; properties of which are given in Table 6.

$$G_R(t) = R_1 + \sum_{n=2}^{N} R_n \exp\left(-t / \frac{\eta_n}{R_n}\right) \tag{1}$$

$$K_R(t) = K_1 + \sum_{n=2}^{N} K_n \exp\left(-t / \frac{\eta_n^K}{K_n}\right) \tag{2}$$

$$K_R(t) = G_R(t) \frac{2(1+\upsilon(t))}{3(1-2\upsilon(t))} \tag{3}$$

$$G_R(\infty) = R_1 \tag{4}$$

$$G_R(0) = R_1 + \sum_{n=2}^{N} R_n \tag{5}$$

$$K_R(\infty) = K_1 \tag{6}$$

$$K_R(0) = K_1 + \sum_{n=2}^{N} K_n \tag{7}$$

$$K_0 = \frac{E_0}{3(1-2\upsilon_0)} \tag{8}$$

$$G(t) = \frac{E(t)}{2(1+\upsilon(t))} \tag{9}$$

Table 4. Elastic layer properties (Helwany et al. 1998, Gopalakrishnan et al. 2006, Johnson et al. 2007, Ullidtz 1987,)

Material	Young's modulus	Poisson's ratio
PCC	27.6 GPa	0.15
HMA	1, 3, 5, 7 GPa	0.35
Base	242 MPa	0.4
Subbase	138 MPa	0.4
Subgrade	52, 70, 100, 120 MPa	0.45

Table 5. Calculated HMA viscoelastic properties

$E(MPa)$	$K(MPa)$	$G_G(MPa)$	$G_R(MPa)$	$\beta(s)$
1000	1111.11	370.37	1000	2.1
3000	3333.33	1111.11	3000	0.7
5000	5555.56	1851.85	5000	0.42
7000	7777.78	2592.59	7000	0.3

Table 6. Drucker-Prager material properties (Gopalakrishnan et al. 2006, Johnson et al. 2007)

Material/Layer	Cohesion (Pa)	Friction angle (degree)
Base	44,100	50
Subbase	34,500	45
Subgrade	160	0.01

Eight-node brick elements were used to model the PCC overlay, base, subbase layers, and subgrade. In order to model the HMA layer with the viscoelastic properties described previously, eight-node brick viscoelastic elements were used that are similar to the eight-node solid element in shape and geometry but different in formulation.

Contact between two surfaces can conveniently be modeled in ANSYS by utilizing the surface-to-surface "contact pairs." Each of these "contact pairs" is capable of representing contact and sliding between 3-D surfaces, with the "target" elements defining the stiffer surface and "contact" elements defining the deformable surface. The interface elements also provide the user with the option of selecting surface interaction models for specific cases such as: "standard," "rough," "no separation," and "bonded." Due to the substantially better performance of bonded overlays in reduction of deflections and stresses in the pavement layers, the "bonded" interaction model was used in this work (Cable 2003, Cable 2005).

The procedure used to model the "half space" subgrade was to find the appropriate cut-off depth for this layer. The appropriate depth in the finite element model is a depth in which the subgrade response to loading (i.e., stresses, deflections, etc.) is negligibly different from that of an infinite subgrade case. A range of subgrade depths starting at 1 m was analyzed, and a 3 m depth was found to be appropriate.

In order to conserve in computational time and expense and due to the large number of 3-D finite element models that had to be analyzed, dowels and tie bars were not modeled explicitly. Instead, a simplified but efficient method was used to model these load transfer devices in which it is assumed that the joints act as linear elastic springs that transfer vertical loads in shear. Hence, the joint model is known as a "linear elastic joint" or "shear spring." Two-node 3-D beam elements were used to model the load transfer mechanism based on the linear elastic joint assumption. In this method, the joint is characterized by an equivalent shear stiffness k_{joint} (David 1998), expressed in units of force per relative vertical displacement per unit length of the joint (N/m/m):

$$K_{joint} = \frac{5EI}{(1+\mu)\delta h^2} \tag{10}$$

Where:
h: Height of the beam element
EI: Required beam stiffness (per unit length of joint)
μ : Poisson ratio for the beam material
δ : Joint width (beam span)

Due to the shear mechanism assumed for the beam elements, the relative vertical displacement caused by loading, induces a shear force V in the beam as well as a moment M at each node. The moment is given by Equation 11:

$$M = V\delta \tag{11}$$

The beam span δ, has to be considered small enough to make the induced moment negligible. Therefore, a value of 2.5 mm was chosen for the joint width that equals the value for the beam height. Figure 2 depicts the 3-D finite element model and its mesh.

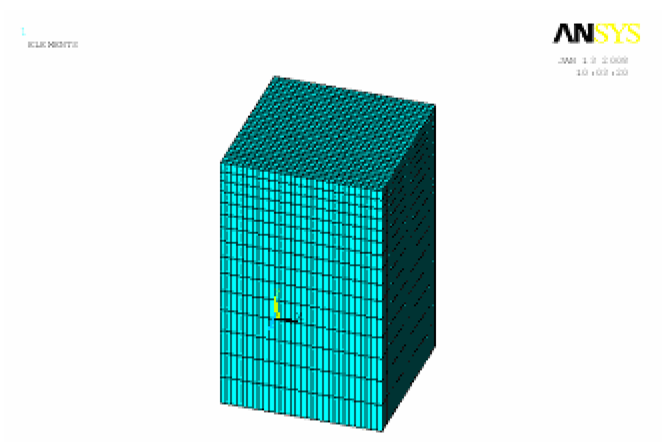

Figure 2. Finite element model for Denver International Airport rigid pavement

The 3-D finite element model dimensions have to be chosen in such a way that the high volume of finite element computations are reduced to an acceptable and optimum level while maintaining the required accuracy and reality in results. A trial-and-error process was applied to find the optimum dimensions for the model. A primary model consisting of 6 (3.6 m by 3.6 m) slabs with 2.8 m shoulders was analyzed first. This took 84 hours using a 3 GHz CPU. The Next step was to slightly shrink the model dimensions (longitudinally and laterally) and analyze the model. The process was resumed up to the point that the results started to vary. Therefore, the optimum model dimensions were determined as follows:

Longitudinal dimension (model length along x axis): (2×3.6+0.01) m
Lateral dimension (model length along z axis): (2×3.6+0.01) m

The overall height of the model could vary based on the chosen thicknesses for each layer. It should be noted that 2.8 m wide concrete shoulders were also considered for the overlay layer.
The primary finite element model and the optimum model can be seen in Figure 3 and Figure 4 respectively.

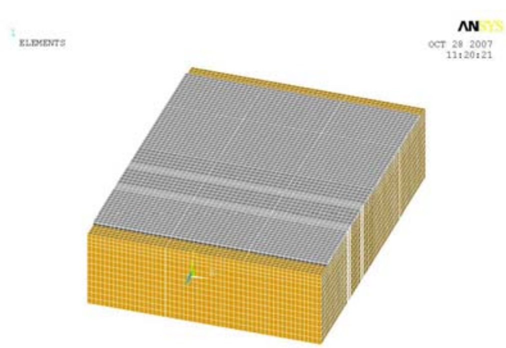

Figure 3. Primary model

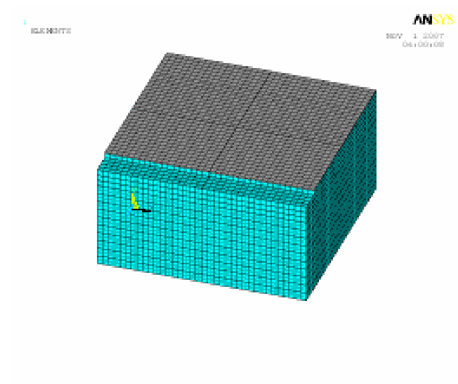

Figure 4. Optimum model

Based on a fair number of models analyzed for finding the optimum dimensions it was seen that the overall thickness of base and subbase layers had a negligible effect on the results; thus, a constant thickness of 200 mm for base and 400 mm for the subbase layers (600mm overall) were used in the analyses. Figure 5 shows the variation of compressive strain on top of the subgrade versus variation of the base and subbase layer thicknesses. Variations of tensile strain at the bottom of the HMA layer against the variation of overall base and subbase layers are indicated in Figure 6.

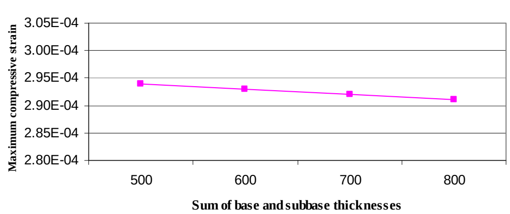

Figure 5. Variations of compressive strain on top of subgrade with base and subbase layer thicknesses

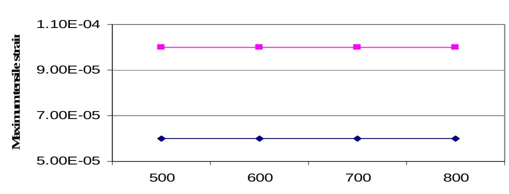

Figure 6. Variations of tensile strain at the bottom of the HMA layer with base and subbase layer thickness

A comparison between deflections on top of the subgrade (Figure 7 and Figure 8) and stresses along the traffic direction (Figure 9 and Figure 10), under the same loading and for the same material properties, between the primary model and the optimized model are depicted in Figure 7 and Figure 8, respectively.

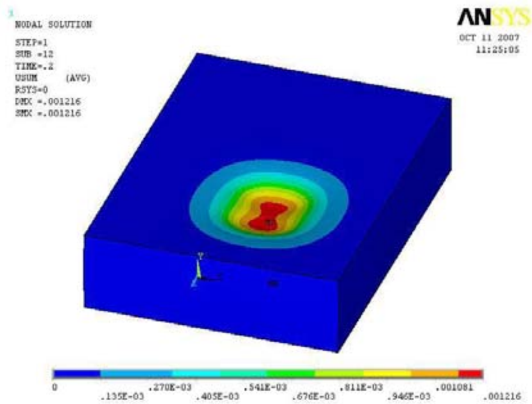

Figure 7. Deflection on top of subgrade in the primary model

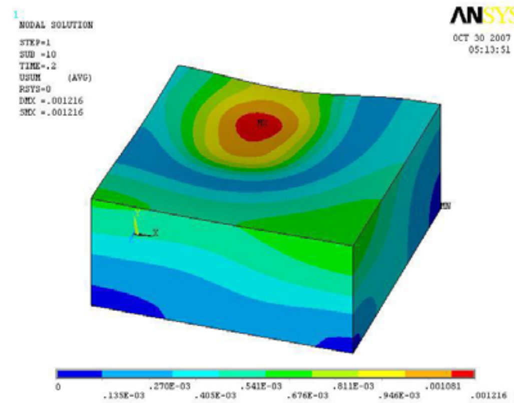

Figure 8. Deflection on top of subgrade in optimum model

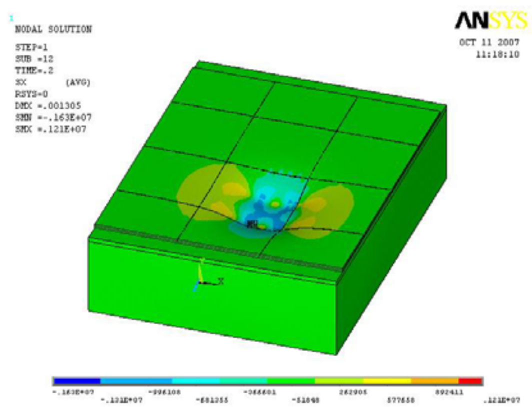

Figure 9. Concrete stress along traffic direction in the primary model

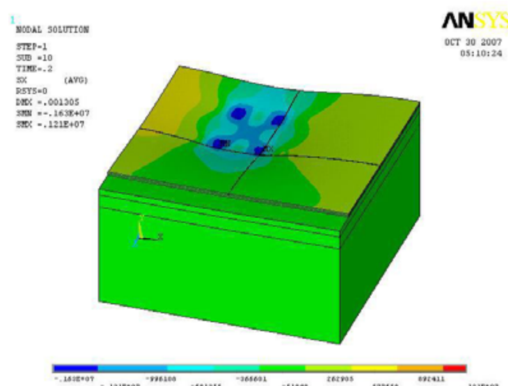

Figure 10. Concrete stress along traffic direction in the optimum model

Design

As many as 1200 finite element models were analyzed with varying thicknesses of the PCC overlay layer, HMA layer, and various Young's moduli for the HMA, as well as different CBR values under 8 axle load groups.

The allowable number of load repetitions were computed using the PCA and NCHRP (NCHRP 2004) fatigue criteria for concrete presented in Equation 12 and 13. The Illinois Department of Transportation fatigue cracking criterion in equation 15 and the Asphalt Institute permanent deformation criterion shown in equation 16 were used to determine the allowable number of load repetitions for the HMA layer (Huang 1993). The smallest of the four governs the design.

$$\log N_f = f_1 - f_2\left(\frac{\sigma}{S_c}\right) \tag{12}$$

$\frac{\sigma}{S_c} \geq 0.55$ $\quad \log N_f = 11.737 - 12.077\left(\frac{\sigma}{S_c}\right)$

$0.45 < \frac{\sigma}{S_c} < 0.55$ $\quad N_f = \left(\frac{4.2577}{\sigma / S_c - 0.4325}\right)^{3.268}$

$\frac{\sigma}{S_c} \leq 0.45$ $\quad N_f = \infty$

$$\log(N_{i,j,k,l,m,n}) = C_1\left(\frac{MR_i}{\sigma_{i,j,k,l,m,n}}\right)^{C_2} + 0.4371 \tag{13}$$

Where:

N : Allowable number of load repetitions

σ : Stress in the concrete

S_c : Concrete modulus of rupture

MR : Concrete modulus of rupture

C_1 and C_2 : Calibration constants, 2 and 1.2 respectively.

And for HMA:

$$N_f = 5\times 10^{-6}(\varepsilon_1)^{-3.0} \tag{14}$$

$$N_d = f_4(\varepsilon_c)^{-f5} \tag{15}$$

Where:

ε_1: Tensile strain at the bottom of the HMA layer

ε_c : Compressive strain on top of the subgrade

$f_4 = 1.365 \times 10^{-9}$

$f_5 = 4.477$

Design Equations

Values obtained from the finite element analyses for maximum stress in the concrete slab, tensile strains at the bottom of the HMA layer in both directions, and compressive strain on top of the subgrade, and values for the HMA Young's modulus, subgrade CBR, thicknesses of the HMA layer and thicknesses of the overlay slabs were used in a number of multiple regressions to obtain prediction equations for a mechanistic design process. Equations to predict maximum stress in the concrete slabs, tensile strains at the bottom of the asphalt layer, and compressive strain at top of subgrade were developed for each axle load group. Predicted values resulting from the equations have to be assessed with respect to fatigue and permanent deformation criteria for HMA as well as fatigue criteria for concrete to obtain the allowable number of load repetitions. Design equations for an 8 ton single-axle load (standard axle) are as follows in equations 16 to 19:

$$\sigma_{PCC} = -58106.33 t_{PCC} - 26844.41 t_{AC} - 14.7 E_{AC} - 13911.65 CBR + 1321319.39$$
$$(R^2 = 0.986) \qquad (16)$$

$$\varepsilon_x \times 10^5 = -0.058 t_{PCC} - 0.475 t_{AC} - 0.001 E_{AC} - 0.02 CBR$$
$$(R^2 = 0.945) \qquad (17)$$

$$\varepsilon_z \times 10^5 = -0.060 t_{PCC} - 0.482 t_{AC} - 0.001 E_{AC} - 0.023 CBR + 12.74$$
$$(R^2 = 0.926) \qquad (18)$$

$$\varepsilon_{compressive} \times 10^5 = -1.326 t_{PCC} - 0.594 t_{AC} - 0.521 CBR + 41.57$$
$$(R^2 = 0.997) \qquad (19)$$

Where:

σ_{PCC} : Maximum stress in the concrete

t_{PCC} : Concrete slab thickness

t_{AC} : HMA layer thickness

E_{AC} : HMA Young's modulus

CBR : California Bearing Ratio for the subgrade soil

ε_x : Tensile strain at the bottom of the HMA layer along the traffic direction

ε_z : Tensile strain at the bottom of the HMA layer perpendicular to the traffic direction

$\varepsilon_{compressive}$: Compressive strain on top of subgrade

Conclusions

- According to the graphs and tables obtained for the allowable number of load repetitions, based on the four criteria discussed previously, it can be seen that in most cases fatigue cracking in the HMA layer governs the design process and not fatigue in the concrete.
- Concrete overlay slabs that structurally act as plates transfer the imposed stress due to loading in a rationally vast domain with low intensity, which causes a fair reduction of the stress transmitted to the HMA layer, which leads to lower tensile strains at the bottom of the layer. Therefore, the concrete overlay considerably enhances load-bearing capacity of the pavement.
- Mechanistic parameters and the allowable number of load repetitions obtained from the analyses indicate that even in seriously damaged pavements under heavy loading, concrete overlays of up to 150 mm thick suffice and in no case an overlay with a greater thickness is required.

References

Abbas, A. R., and Papagiannakis, A. T., and Masad, E. A. (2004). "Linear and Nonlinear Viscoelastic Analysis of the Microstructure of Asphalt Concretes." *J. Mat. Civil. Eng.,* ASCE 16(2), 133-139.

ANSYS Users Manuals. South Point, Canonsburg, PA, USA: Ansys, Inc.; 1999.

Burnham, T., and D. Rettner (2003). "Whitetopping and Hot-Mix Asphalt Overlay Treatments for Flexible Pavements", Maplewood, MN: Minnesota Department of Transportation.

Cable, J.k., Anthony, M. L., Fanous, F.S., and Pahres, B.M. (2003). *Evaluation of Composite Pavement Unbonded Overlays: Phases I and II.*, Ames, IA: Iowa State University, Center for Portland Cement Concrete Pavement Technology.

Cable, J.K., Fanous F. S., Ceylan, H., Wood, D., Daniel, F., Tabbert, T., Oh, S. Y., and Gopalakrishnan, K. (2005). *Design and Construction Procedures for Concrete Overlay and Widening of Existing Pavements.*, Final Report (2005), Iowa State University.

David, R. B. (1998). *Development of Advanced Computational Models for Airport Pavement Design.*, DOT/FAA/AR-97/47., Federal Aviation Administration, Washington DC.

Gopalakrishnan K. and Thompson M. R., (2006). "Assessing Damage to Airport Pavement Structure due to Complex Gear Loads" *J. Trans. Eng.,* ASCE 132(11), 888-897.

Helwany S., Dyer J. and Leidy J. (1998), "Finite Element Analysis of Flexible Pavements" *J. Trans. Eng.,* ASCE 124(5), 491-499.

Huang, Y. H. (1993). Pavement Analysis and Design. Prentice Hall.

Johnson D., Sukumaran B., Mehta Y. and Willis, M. (2007). “Three Dimensional Finite Element Analysis of Flexible Pavements to Assess the Effects of Wander and Wheel Configuration” *Proc. 2007 FAA Worldwide Airport Technology Transfer Conference.* Atlantic City, New Jersey, USA.

National Cooperative Highway Research Program. 2004. Guide for Mechanistic-Empirical Design of New and Rehabilitated Pavement Structures. Washington DC: Transportation Research Board, National Research Council.

Ullidtz, P. (1987), Pavement Analysis, Oxford, New York.